Bandwidth Control of Optimized FDTD Schemes

Theodoros T. Zygiridis

Department of Informatics and Telecommunications Engineering
University of Western Macedonia, Kozani 50100, Greece
tzygiridis@uowm.gr

Abstract ─ We investigate the potential of controlling the wideband behavior of finite-difference time-domain (FDTD) methods, which adopt extended spatial operators while maintaining the standard temporal updating procedure. Specifically, single-frequency optimization is performed first, while wider bands are then treated with the aid of the least-squares technique. The proposed methodology is applied to various discretization schemes with different stencil sizes and shapes, thus verifying its versatile character. Theoretical as well as numerical results are presented, which demonstrate that the optimization process has a beneficial impact on the efficiency of FDTD algorithms, and yields attractive alternatives for reliable multi-frequency simulations.

Index Terms ─ Finite-difference time-domain (FDTD) methods, high-order schemes, least squares, performance optimization.

I. INTRODUCTION

When solving wideband electromagnetic problems, a common feature in Yee's finite-difference time-domain (FDTD) method [1-4] and other standard techniques is that low-frequency components are modeled more reliably than those at higher frequencies. This phenomenon is due to the use of finite-difference operators that originate from truncated Taylor series. Experience has shown that such general approximations do not necessarily produce the lowest errors. In addition, Taylor-based schemes may be inefficient, when different orders of spatial and temporal differencing are combined. For instance, to ensure adequate performance for the (2,4) FDTD method, one should use significantly smaller time steps, compared to the stability limit [5]. On the other hand, a class of computational alternatives comprises schemes that exhibit optimized behavior, even if their formal accuracy order is not maximized. In contrast with conventional solutions, their frequency response is adjustable to problem-related needs. Usually, single-frequency optimization is realized [6–9], which cannot always ensure satisfactory wideband characteristics or control of the optimization bandwidth. Yet, there exist approaches that directly deal with the challenging issue of multi-frequency error control. For instance, one-dimensional suppression of phase errors, integrated over the wavenumbers of practical interest, is proposed in [10]. Another choice is to minimize numerical dispersion at one frequency, while applying additional constraints to the finite-difference coefficients [11]. The algorithms presented in [12, 13] accomplish their goals by introducing frequency-dependent quantities in the update equations, eventually altering the size of the operator stencil. Another solution [14] combines error reduction at selected wavelengths and directions of propagation. Note that we will not be concerned with inaccuracies due to geometric modeling, which can be handled with other approaches, such as subgridding techniques [15, 16].

In the present study, we focus on FDTD approaches that preserve the time advancing of Yee's method, so practically only the spatial-differencing process is modified (yet, it is shown that high convergence rates are still feasible). In order to remedy algorithmic reliability over extended frequency bands, we exploit the fact that optimum performance – according to a specific criterion – can be ensured at one frequency point. In essence, after determining a consistent error

formula, single-frequency correction is translated into a set of linear equations. The unknowns in these equations are constant coefficients, introduced by the spatial operators. An augmented system is formulated afterwards, by repeating this procedure for a number of frequency points within the band of interest. The new system is overdetermined; hence, it is solved approximately with the least-squares method. Being generalized, the proposed formulation is applied to five discretization schemes, leading to different levels of reliability. The dispersion and anisotropy flaws of the modified approaches are examined theoretically, and numerical simulations are executed to demonstrate the qualities of the new techniques.

II. METHODOLOGY

A. The case of $(2,2N)$ schemes

The present study is concerned with the two-dimensional Maxwell's equations. In the first case examined, partial derivatives with respect to space variable u ($u = x, y$) are approximated at point $i\Delta u$ by the parametric operator

$$\mathrm{D}_u\left[f_i\right]=\frac{1}{\Delta u}\sum_{\ell=1}^{N}C_\ell\left(f_{i+\frac{2\ell-1}{2}}-f_{i-\frac{2\ell-1}{2}}\right). \qquad (1)$$

In this expression, the number of considered field samples is $2N$, N = 1, 2, 3, and the unknown C_ℓ coefficients are determined later. As mentioned in the introduction, time marching is performed using the second-order leapfrog scheme:

$$\mathrm{D}_t\left[f^n\right]=\frac{1}{\Delta t}\left(f^{n+\frac{1}{2}}-f^{n-\frac{1}{2}}\right). \qquad (2)$$

Thus, the updating procedure is similar to that of the classic FDTD method. For instance, the H_z component is updated according to

$$H_z\Big|_{i+\frac{1}{2},j+\frac{1}{2}}^{n+\frac{1}{2}}=H_z\Big|_{i+\frac{1}{2},j+\frac{1}{2}}^{n-\frac{1}{2}}+\frac{\Delta t}{\mu_0}\left(\mathrm{D}_y\left[E_x\Big|_{i+\frac{1}{2},j+\frac{1}{2}}^{n}\right]-\mathrm{D}_x\left[E_y\Big|_{i+\frac{1}{2},j+\frac{1}{2}}^{n}\right]\right). \qquad (3)$$

We label these algorithms $(2,2N)$, indicating the temporal/spatial structure of the corresponding discretization scheme. The key idea is to reduce the inherent error as isotropically as possible at one frequency, and then tune the operators' response within wider bands. To exemplify the derivation of the x-operator, we start from the equation

$$\varepsilon\frac{\partial E_y}{\partial t}+\frac{\partial H_z}{\partial x}=0. \qquad (4)$$

Admitting plane-wave forms similar to the exact solutions for both field components in the discrete form of (4) yields

$$\epsilon\left(\omega,\tilde{k},\varphi\right)=\frac{\Delta x}{c_0\Delta t}\sin\left(\frac{\omega\Delta t}{2}\right)\cos\phi-\sum_{\ell=1}^{N}C_\ell\sin\left(\frac{2\ell-1}{2}\tilde{k}_x\Delta x\right)=0, \qquad (5)$$

where $\tilde{k}_x=\tilde{k}\cos\phi$ is the x-component of the numerical wavenumber $\tilde{k}$, and ϕ denotes the propagation angle. If $\tilde{k}=k=\omega/c_0$ is additionally enforced, then (5) does not remain valid, as numerical and exact wavenumbers do not coincide in general, due to discretization artifacts. Nevertheless, given that $\epsilon(\omega,k,\phi)=0$ corresponds to the ideal scenario of an error-free algorithm, an acceptable representation of the continuous problem should be feasible, as long as C_ℓ values that render $\epsilon(\omega,k,\phi)$ close to zero are selected. We refrain from specifying individual values for ϕ, since all directions can be treated rather equally, by exploiting the error's trigonometric expansion:

$$\epsilon\left(\omega,k,\varphi\right)=\frac{\Delta x}{c_0\Delta t}\sin\left(\frac{\omega\Delta t}{2}\right)\cos\phi-2\sum_{\ell=1}^{N}C_\ell\sum_{i=0}^{\infty}(-1)^i J_{2i+1}\left(\tfrac{2\ell-1}{2}k\Delta x\right)\cos\left[(2i+1)\phi\right]. \qquad (6)$$

Evidently, small values for ϵ can be easily accomplished at a designated angular frequency ω_0 through the vanishing of the first N terms in (6). In this way, a $N\times N$ system of equations is formed,

$$\left[a_{ij}(\omega_0)\right]\left[\mathrm{C}\right]=\left[b_i(\omega_0)\right], \qquad (7)$$

where

$$a_{ij}=J_{2i-1}\left(\frac{2j-1}{2}\frac{\omega\Delta x}{c_0}\right)\quad(1\le i,j\le N) \qquad (8)$$

$$b_1=\frac{\Delta x}{c_0\Delta t}\sin\left(\frac{\omega\Delta t}{2}\right) \qquad (9)$$

$$b_i=0\quad(i\ne 1), \qquad (10)$$

$J_n(x)$ denotes Bessel functions of the first kind, and [C] is the vector of the C_ℓ coefficients. As expected, the C_ℓ values calculated from (7) depend on spatial as well as temporal increments. For instance, the two necessary equations in the case of the $(2,4)$ scheme are:

$$\begin{bmatrix} J_1(\frac{k\Delta x}{2}) & J_1(\frac{3k\Delta x}{2}) \\ J_3(\frac{k\Delta x}{2}) & J_3(\frac{3k\Delta x}{2}) \end{bmatrix} \begin{bmatrix} C_1 \\ C_2 \end{bmatrix} = \begin{bmatrix} \frac{\Delta x}{2c_0\Delta t}\sin(\frac{\omega\Delta t}{2}) \\ 0 \end{bmatrix}. \quad (11)$$

Given that the described procedure relies on the selection of a specific frequency ω_0, it is expected that error decrease will be confined to the corresponding part of the spectrum. To pursue a more wideband performance tuning, we propose the application of a least-squares approach. Let's assume that the band of interest is described by $\omega_{\min} \le \omega \le \omega_{\max}$. Then, an extended set of equations can be derived by introducing a partition $\Omega = \{\omega_1, \omega_2, \ldots, \omega_M\}$ of the interval $[\omega_{\min}, \omega_{\max}]$. For each point $\omega_i \in \Omega$ ($i = 1, \ldots, M$), the corresponding equations from (7) are obtained, and all of them are assembled, in order to build a new – overdetermined – system:

$$[\mathcal{A}][\mathrm{C}] = [\mathcal{B}], \quad (12)$$

where

$$[\mathcal{A}] = \begin{bmatrix} [a_{ij}(\omega_1)] \\ [a_{ij}(\omega_2)] \\ \vdots \\ [a_{ij}(\omega_M)] \end{bmatrix}, \quad [\mathcal{B}] = \begin{bmatrix} [b_i(\omega_1)] \\ [b_i(\omega_2)] \\ \vdots \\ [b_i(\omega_M)] \end{bmatrix}. \quad (13)$$

An approximate solution to (12) is calculated by applying the least-squares method:

$$[\mathrm{C}] \simeq \left([\mathcal{A}]^{\mathrm{T}}[\mathcal{A}]\right)^{-1}\left([\mathcal{A}]^{\mathrm{T}}[\mathcal{B}]\right). \quad (14)$$

The operators acquired in this way are expected to perform well, within the prescribed band.

It is noted that the case of *y*-operators can be handled in the same manner, starting from

$$\varepsilon\frac{\partial E_x}{\partial t} - \frac{\partial H_z}{\partial y} = 0. \quad (15)$$

B. The case of $(4,2N)$ schemes

From the above description it appears that the generalized character of the proposed methodology permits further applications. Therefore, we extend the optimization procedure to FDTD schemes, which practically adopt a modified version of the fourth-order leapfrog integrator [17]. Recall that time integration based on the fourth-order leapfrog approach introduces temporal operators with the following form:

$$\mathrm{D}_t[f^n] = \frac{f^{n+\frac{1}{2}} - f^{n-\frac{1}{2}}}{\Delta t} - \frac{\Delta t^2}{24}\mathrm{D}_t^{(3)}[f^n], \quad (16)$$

where $\mathrm{D}_t^{(3)}$ stands for a second-order approximation of the third-order temporal derivative, calculated with the proper use of spatial formulae. It can be easily shown that the structure of such algorithms is equivalent to a combination of the standard second-order leapfrog scheme with extended, two-dimensional, spatial operators. We denote these algorithms as $(4,2N)$, N = 2, 3, and the geometric configuration of their spatial expressions can be identified in Fig. 1. Analytically, the parametric expression of the D_x operator now becomes

$$\mathrm{D}_x\left[f_{i,j}\right] = \frac{1}{\Delta x}\sum_{\ell=1}^{N} C_\ell\left(f_{i+\frac{2\ell-1}{2},j} - f_{i-\frac{2\ell-1}{2},j}\right) + \frac{1}{\Delta x}C_{N+1}\left(f_{i+\frac{1}{2},j+1} + f_{i+\frac{1}{2},j-1} - f_{i-\frac{1}{2},j+1} - f_{i-\frac{1}{2},j-1}\right). \quad (17)$$

Compared to the formula in (1), an extra degree of freedom has been added (C_{N+1}), which weights nodal values appearing on both sides of the differentiation axis. Following the methodology applied to $(2,2N)$ schemes, we define a similar error expression, whose trigonometric expansion is

$$\epsilon(\omega,k,\phi) = \frac{\Delta x}{c_0\Delta t}\sin\left(\frac{\omega\Delta t}{2}\right)\cos\phi - 2\sum_{\ell=1}^{N} C_\ell\sum_{i=0}^{\infty}(-1)^i J_{2i+1}\left(\tfrac{2\ell-1}{2}k\Delta x\right)\cos\left[(2i+1)\phi\right] - 4C_{N+1}\sum_{i=0}^{\infty}(-1)^i J_{2i+1}\left(\tfrac{k\Delta\chi}{2}\right)\cos\left[(2i+1)\phi_0\right]\cos\left[(2i+1)\phi\right],$$

where

$$\Delta\chi = \sqrt{4(\Delta x)^2 + (\Delta y)^2}, \ \tan\phi_0 = 2\Delta x/\Delta y. \quad (18)$$

Now, a $(N+1)\times(N+1)$ system is formulated by zeroing the first $(N+1)$ error terms. For example, we give the three necessary equations for the single-frequency design of the (4,4) scheme:

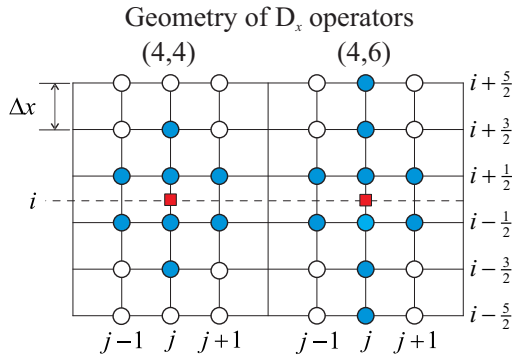

Fig. 1. Nodal arrangement of the operators used for spatial differencing by the $(4,2N)$ schemes.

$$\begin{bmatrix} J_1(\frac{k\Delta x}{2}) & J_1(\frac{3k\Delta x}{2}) & 2J_1(\frac{k\Delta \chi}{2})\cos\phi_0 \\ J_3(\frac{k\Delta x}{2}) & J_3(\frac{3k\Delta x}{2}) & 2J_3(\frac{k\Delta \chi}{2})\cos 3\phi_0 \\ J_5(\frac{k\Delta x}{2}) & J_5(\frac{3k\Delta x}{2}) & 2J_5(\frac{k\Delta \chi}{2})\cos 5\phi_0 \end{bmatrix} \begin{bmatrix} C_1 \\ C_2 \\ C_3 \end{bmatrix} = \begin{bmatrix} \frac{\Delta x}{2c_0\Delta t}\sin(\frac{\omega\Delta t}{2}) \\ 0 \\ 0 \end{bmatrix}. \quad (19)$$

Then, the wideband optimization is carried out with the application of the least-squares method, as presented in detail in Section II-A.

III. THEORETICAL ASPECTS

For simplicity, we assume $\Delta x = \Delta y = \Delta h$. In the case of the $(4,2N)$ schemes, the stability criterion is described by

$$\Delta t \le \frac{\Delta h}{c_0\sqrt{2}\left(\sum_{\ell=1}^{N}|C_\ell| - 2C_{N+1}\right)}, \quad (20)$$

while the corresponding numerical dispersion relation, which will be utilized later for theoretical tests, is

$$\left(\frac{\Delta h}{c_0\Delta t}\right)^2 \sin^2\left(\frac{\omega\Delta t}{2}\right) = \mathcal{X}^2 + \mathcal{Y}^2, \quad (21)$$

where

$$\mathcal{X} = \sum_{\ell=1}^{N} C_\ell \sin\left(\frac{2\ell-1}{2}\tilde{k}\cos\phi\Delta h\right) + 2C_{N+1}\sin\left(\frac{1}{2}\tilde{k}\cos\phi\Delta h\right)\cos\left(\tilde{k}\sin\phi\Delta h\right) \quad (22)$$

$$\mathcal{Y} = \sum_{\ell=1}^{N} C_\ell \sin\left(\frac{2\ell-1}{2}\tilde{k}\sin\phi\Delta h\right) + 2C_{N+1}\sin\left(\frac{1}{2}\tilde{k}\sin\phi\Delta h\right)\cos\left(\tilde{k}\cos\phi\Delta h\right). \quad (23)$$

Formulae (20)-(23) apply in the case of $(2,2N)$ schemes as well, considering that it is $C_{N+1} = 0$ for those algorithms. Hereafter, the time-step size is described by Q, where $Q = \sqrt{2}c_0\Delta t / \Delta h$. Note that the maximum value of Q is 1 for the standard (2,2) and (4,4) techniques, 6/7 for the standard (2,4) and 120/149 for the standard (2,6) scheme. To assess algorithmic accuracy via the numerical phase velocity $\tilde{c}$, the following error definition is used,

$$\mathcal{E}(\omega) = \frac{1}{2\pi c_0}\int_0^{2\pi}\left|c_0 - \tilde{c}(\omega,\phi)\right| d\phi, \quad (24)$$

which is a measure of the mean-error value for all possible propagation angles.

Starting from $(2,2N)$ algorithms, the variation of $\mathcal{E}$ as a function of the grid density is illustrated in Figs. 2(a)-(c). We consider two different cases: in the first one, the band of interest ranges from 25 to 35 cells per wavelength, and from 20 to 40 cells per wavelength in the second case. When $N = 1$ (Q = 0.99 is selected for the optimized techniques), moderate error reduction can be noted. On the other hand, substantial improvement is obtained when N = 2 (Q = 0.85), and even more precise results are observed in the case of six-point operators (Q = 0.7). The latter value of Q is selected due to stability purposes. As deduced from these examples, the accomplished accuracy amendment tends to concentrate toward smaller wavelengths. This is deemed a desirable feature, for high-frequency inaccuracies have the most serious impact.

Next, the $(4,2N)$ schemes are investigated in a similar fashion. Now, the desired frequency band corresponds to 30-60 cells per wavelength, and the calculated error curves appear in Fig. 3. We can verify that the modified leapfrog integration leads to smaller error fluctuations within the prescribed frequency band. In addition, it can be safely concluded that the extra degree of freedom provided by the (4, 6) scheme, compared to the (4, 4) counterpart, allows further upgrade.

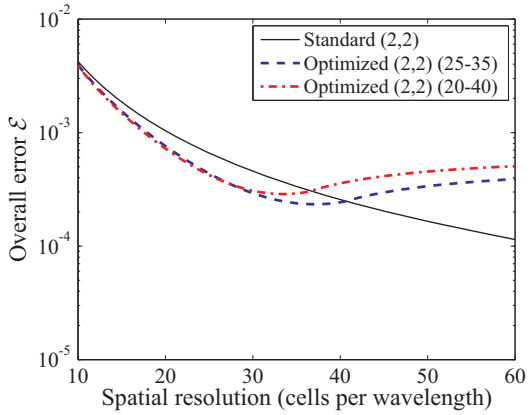

(a)

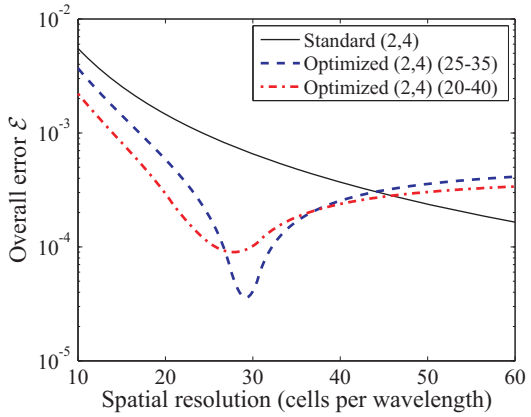

(b)

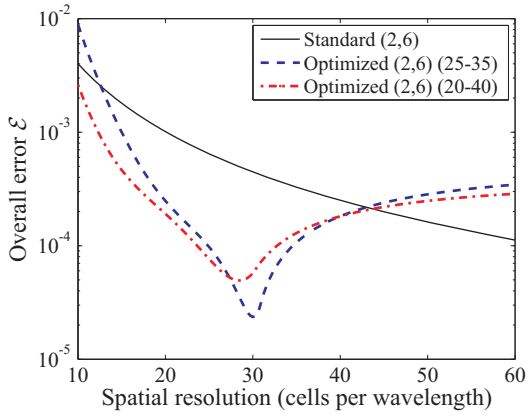

(c)

Fig. 2. Error $\mathcal{E}$ versus spatial grid resolution for $(2,2N)$ schemes: (a) $N=1$, (b) $N=2$, (c) $N=3$. Optimization is performed within either 25-35 or 20-40 cells per wavelength.

As mentioned in the introduction, a known property of schemes with lower temporal than spatial error (such as the standard (2,4) method) is the capability to improve their performance, when small time-step sizes (down to a specific limit) are selected. It is now examined whether the optimized (4, 6) technique exhibits an improved response, provided that small values for Δt are used. If we refer to Fig. 4, we may verify that this distinct feature is exhibited by the optimized (4,6) scheme as well, since a denser temporal sampling can lead to a quite equally distributed error suppression over the designated frequencies of interest.

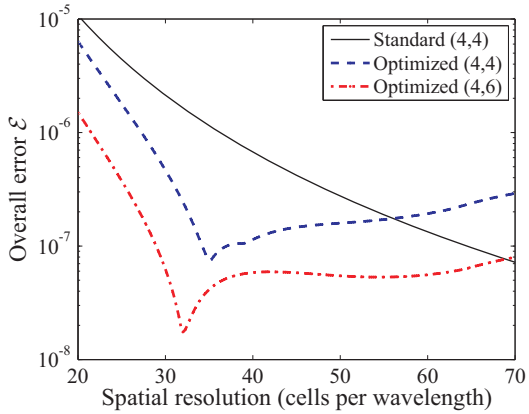

Fig. 3. Error $\mathcal{E}$ versus spatial resolution, in the case of the (4,4) and (4,6) schemes. The optimization bandwidth is 30-60 cells per wavelength.

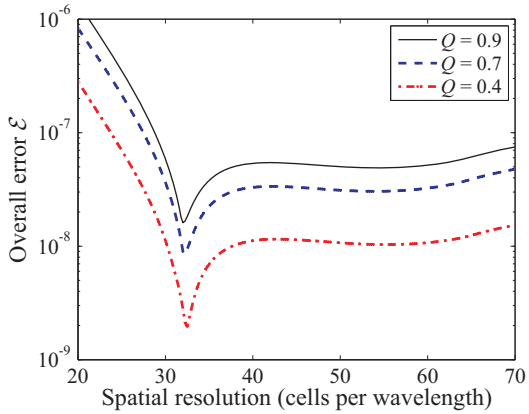

Fig. 4. Error $\mathcal{E}$ versus spatial resolution for varying time-step size, in the case of the (4,6) scheme.

IV. NUMERICAL RESULTS

In the first examples, the performance of $(2,2N)$ schemes is investigated. We initially test the narrowband optimization ensured by (7)-(10), by calculating the maximum L_2 error regarding the H_z component, when single-mode excitation is enforced in a 10 cm × 5 cm rectangular cavity with

perfectly conducting boundaries. The selected mode is TE_{22}, with a resonant frequency of 6.704 GHz. Standard as well as optimized techniques are tested considering grids with different resolutions, and the results are presented in Fig. 5. It is noted that maximum allowable time steps are selected in all cases. As anticipated, the Taylor-based algorithms exhibit second-order behavior even when extended stencils are utilized, as their low temporal accuracy dominates. On the other hand, the optimization practice treats the combined space-time errors efficiently, hence resulting in higher convergence rates. For reference, we mention that when $\Delta h = 0.568$ mm, the computational times for $N = 2, 4, 6$ is 48.8, 57.3, and 62.4 sec, respectively.

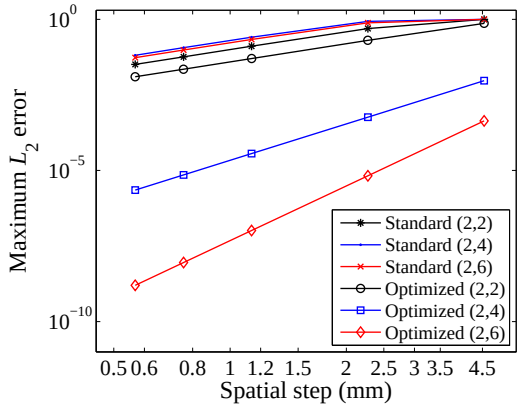

Fig. 5. Maximum L_2 error versus spatial-step size in the cavity problem with single-mode excitation.

Next, multi-modal excitation is introduced into the cavity of the previous example. Specifically, the excited modes are: TE_{11} at 3.352 GHz, TE_{31} at 5.405 GHz, and TE_{12} at 6.181 GHz. Now, the wideband optimization based on the least-squares approach is applied. The results depicted in Fig. 6 are consistent with the theoretical findings, and indicate that all schemes converge at a second-order rate (maximum time steps are again chosen). The level of error reduction in the case of Yee's method is approximately 25%. When $N = 2$, the performance upgrade appears more considerable, as 10-time lower errors are produced, compared to the conventional solution. The wideband (2, 2) and (2, 4) schemes produce the same computational times as the standard ones (9.1 and 11.3 sec, respectively, when $\Delta h = 1.14$ mm). Even better results are computed when $N = 3$; yet, the six-point operators call for reduced time steps when finer lattices are considered, which slightly increase the computational burden. Specifically, the simulation time increases from 12.5 sec to 18.9 sec, when $\Delta h = 1.14$ mm. Nevertheless, the accuracy gain is high, and the optimized (2,6) algorithm remains more efficient than the standard version.

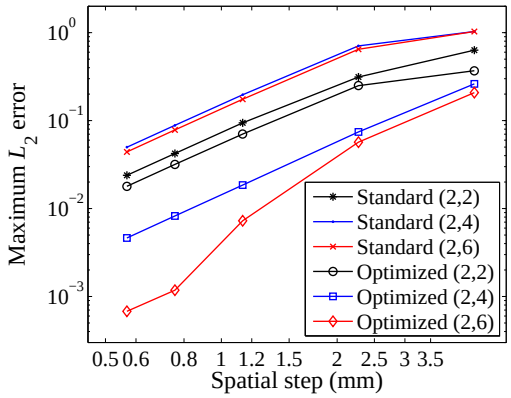

Fig. 6. Maximum L_2 error versus spatial-step size in the cavity problem with multi-modal excitation.

We, also, investigate the achievable rates of convergence, when the errors due to the low-order leapfrog updating are controlled with the use of sufficiently small time steps. For instance, the standard (2, 4) method can be fourth-order accurate, provided that the reduction of Δh by a factor of α is combined with a time-step reduction by α^2. We use the previous numerical test to determine whether the new (2, 4) and (2, 6) algorithms possess this property as well. As illustrated in Fig. 7, high convergence rates (consistent with the size of the spatial stencil) are recovered for standard as well as optimized schemes. Yet, the latter exhibit extra accuracy enhancement, which is estimated close to a factor of 10 in this example.

Proceeding with the $(4,2N)$ techniques, a 50 cm × 5 cm parallel-plate waveguide is modeled. In this configuration, three different modes are excited: TM_1 at 4.5 GHz, TM_2 at 7.5 GHz, and TM_3 at 10.5 GHz. The accuracy of various schemes is tested with grids of 200 × 20 cells, 400 × 40 cells, and 800 × 80 cells. Comparisons are made against the standard (4, 4) method. The results shown in Table 1 verify fourth-order convergence in all cases. However, error improvement by 6.8 and 8.8 times is reported, when the standard (4, 4) method is compared to the optimized (4, 4) and (4, 6) algorithms, respectively. In the case of the denser grid,

the computational time is practically the same for the standard and optimized (4,4) schemes, while the wideband (4,6) method slightly increases the simulation's duration by approximately 6 %, due to smaller time step.

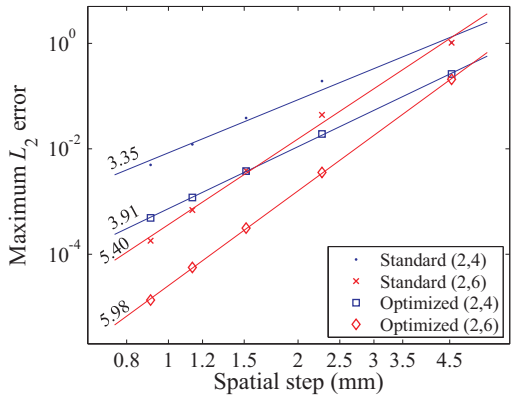

Fig. 7. Maximum L_2 error versus spatial-step size in the cavity problem with multi-modal excitation, when sufficiently small time steps are used. The convergence rates are also shown.

Table 1: Maximum L_2 errors in the parallel-plate waveguide problem

Δh (mm)	Standard (4,4)	Opt. (4,4)	Opt. (4,6)
2.5	3.15e–5	4.61e–6	3.72e–6
1.25	1.98e–6	2.88e–7	2.25e–7
0.625	1.24e–7	1.80e–8	1.39e–8

In the last test, a 5 cm × 5 cm cavity is considered, whose resonant frequencies within the band 2.998 GHz – 18.961 GHz are detected. The selected mesh comprises 25 × 25 cells, and the total simulation time corresponds to 131,072 time steps. A sufficiently narrow Gaussian pulse is used for the introduction of electromagnetic energy in the cavity. The errors concerning the $(2,2N)$ methods are shown in Fig. 8a, while Fig. 8b plots the corresponding error curves in the case of the $(4,2N)$ schemes. Moreover, an explicit reference to the numerical error values is made in Table 2. As seen, the theoretically predicted wideband upgrade of the algorithms' performance is verified, as high-frequency components are now modeled in a more reliable fashion. Note that the error of the optimized (4,6) scheme is dictated by the resolution of field samples in the frequency domain, rather than the – highly accurate – discretization process.

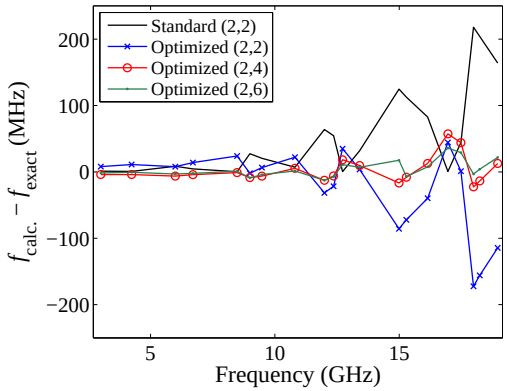

(a)

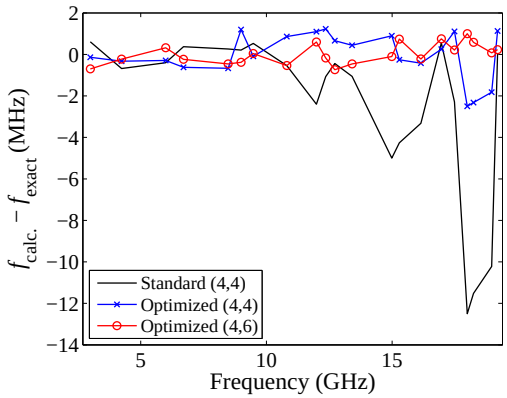

(b)

Fig. 8. Errors in the calculation of a cavity's resonant frequencies: (a) $(2,2N)$ schemes, (b) $(4,2N)$ schemes.

Table 2: Errors of various algorithms in the detection of a cavity's resonant frequencies

Method	$\max\{\lvert\Delta f\rvert\}$ (MHz)	$\max\left\{\frac{\lvert\Delta f\rvert}{f_{exact}}\right\}\cdot 100\%$
Standard (2,2)	217.9	1.21
Opt. (2,2)	172.4	0.96
Opt. (2,4)	57.35	0.34
Opt. (2,6)	35.95	0.21
Standard (4,4)	12.5	0.069
Opt. (4,4)	2.5	0.014
Opt. (4,6)	1	0.023

V. CONCLUSION

We have presented a systematic methodology that facilitates performance control of FDTD approaches over a selected frequency range. It has been pointed out, both theoretically and computationally, that algorithms based on the leapfrog integrator can be optimized within designated frequency bands, by solving an over determined sys-

tem with the least-squares method. In this way, FDTD schemes with $(2,2N)$ structure have been rendered efficient, even when operated close to stability limits. Moreover, high-order convergence has been exhibited by optimized $(4,2N)$ techniques in multi-frequency problems, ensuring improvement over standard counterparts. Compared to classic analogues, the new operators suppress errors in a broadband fashion, without extra computational burden. The proposed practice is generic and can be applied to several FDTD schemes, as long as the proper error analysis is performed.

REFERENCES

[1] K. S. Yee, "Numerical solution of initial boundary value problems involving Maxwell´s equations in isotropic media," *IEEE Trans. Antennas Propag*., vol. 14, pp. 302-307, 1966.

[2] A. Taflove and M. E. Brodwin, "Numerical solution of steady-state electromagnetic scattering problems using the time-dependent Maxwell's equations," *IEEE Trans. Microw. Theory Tech.*, vol. 23, no. 8, pp. 623-630, Aug. 1975.

[3] A. Taflove, "Application of the finite-difference time-domain method to sinusoidal steady-state electromagnetic-penetration problems," *IEEE Trans. Electromagn. Compat.*, vol. 22, no. 3, pp. 191-202, Aug. 1980.

[4] A. Taflove and S. C. Hagness, *Computational Electrodynamics: The Finite-Difference Time-Domain Method, 3rd ed.* Norwood, MA: Artech House, 2005.

[5] A. Yefet and P. G. Petropoulos, "A staggered fourth-order accurate explicit finite difference scheme for the time-domain Maxwell's equations," *J. Comput. Phys.*, vol. 168, pp. 286–315, 2001.

[6] J. B. Cole, "A high-accuracy realization of the Yee algorithm using non-standard finite differences," *IEEE Trans. Microw. Theory Tech.*, vol. 45, no. 6, pp. 991-996, June 1997.

[7] E. A. Forgy and W. C. Chew, "A time-domain method with isotropic dispersion and increased stability on an overlapped lattice*," IEEE Trans. Antennas Propag.*, vol. 50, no. 7, pp. 983-996, July 2002.

[8] I.-S. Koh, H. Kim, J.-M. Lee, J.-G. Yook, and C. S. Pil, "Novel explicit 2-D FDTD scheme with isotropic dispersion and enhanced stability," *IEEE Trans. Antennas Propag.*, vol. 54, no. 11, pp. 3505-3510, Nov. 2006.

[9] A.-X. Zhao, B.-K. Huang, and W.-B Wang, "Study of low-dispersion ADI-FDTD method with isotropic finite difference," *IEEE Antennas Wireless Propag. Lett.*, vol. 8, pp. 275-278, 2009.

[10] C. K. W. Tam and J. C. Webb, "Dispersion-relation-preserving finite difference schemes for computational acoustics," *J. Comput. Phys.*, vol. 107, no. 2, pp. 262-281, 1993.

[11] H. E. A. El-Raouf, E. A. El-Diwani, A. El-Hadi Ammar, and F. M. El-Hefnawi, "A FDTD hybrid "$M3d_{24}$" scheme with subgridding for solving large electromagnetic problems," *ACES Journal*, vol. 17, no. 1, pp. 23-29, Mar. 2002.

[12] S. Wang and F. L. Teixeira, "Dispersion-relation-preserving FDTD algorithms for large-scale three-dimensional problems," *IEEE Trans. Antennas Propag.*, vol. 51, no. 8, pp. 1818–1828, Aug. 2003.

[13] T. Ohtani, K. Taguchi, T. Kashiwa, Y. Kanai, and J. B. Cole, "Nonstandard FDTD method for wide-band analysis," *IEEE Trans. Antennas Propag.*, vol. 57, no. 8, pp. 2386–2396, Aug. 2009.

[14] Y. Liu and M. K. Sen, "A new time-space domain high-order finite-difference method for the acoustic wave equation," *J. Comput. Phys.*, vol. 228, no. 23, pp. 8779-8806, 2009.

[15] P. Monk, "Sub-gridding FDTD schemes," *ACES Journal*, vol. 11, no. 1, pp. 37-46, Mar. 1996.

[16] S. Wang, "Numerical examinations of the stability of FDTD subgridding schemes," *ACES Journal*, vol. 22, no. 2, pp. 189-194, July 2007.

[17] H. Spachmann, R. Schuhmann, and T.Weiland, "Higher order time integration schemes for Maxwell's equations," *Int. J. Numerical Modeling: Electron. Networks, Devices and Fields*, vol. 15, pp. 419–437, 2002.

Theodoros T. Zygiridis received the Diploma and Ph.D. degrees in Electrical and Computer Engineering from Aristotle University of Thessaloniki, Greece, in 2000 and 2006, respectively. He is now a Lecturer at the Department of Informatics and Telecommunications Engineering, University of Western Macedonia, Greece. His research interests lie in the area of Computational Electromagnetics, and currently focus on finite-difference time-domain algorithms, high-order techniques, and dispersion-relation-preserving methodologies.